Packing-Density Effects on the Friction of *n*-Alkane Monolayers

Paul T. Mikulski and Judith A. Harrison*

Contribution from the Department of Chemistry, United States Naval Academy, Annapolis, Maryland 21402

Received January 23, 2001

Abstract: The classical molecular dynamics simulations presented here examine the tribology associated with the sliding of a hydrogen-terminated diamond counterface across a monolayer of *n*-alkane chains that are covalently bound to a diamond substrate. Two systems using chains of fixed length (18 carbon atoms per chain) on diamond (111) are examined: a tightly packed (2×2) arrangement and a loosely packed system with approximately 30% fewer chains. Both systems give a similar average friction at low loads. Under high loads, the tightly packed monolayer exhibits significantly lower friction than the loosely packed monolayer. While the movement of chains is greatly constricted in both systems, the tightly packed monolayer under high loads is clearly more uniform in geometry and more constrained with respect to the movement of individual chains than the loosely packed monolayer. This suggests that efficient packing of the chains is responsible for the lower friction for tight packing under high load. This is supported by the fact that sliding initiates larger bond-length fluctuations in the loosely packed system, which ultimately lead to more energy dissipation via vibration.

Introduction

As the dimensions of micromachines steadily decrease, the magnitudes of the surface forces in the machine increase in importance. There exists some critical distance where the dimensions of the parts involved are not large enough to prevent surface forces from causing parts to stick together (a phenomenon known as stiction).[1] To overcome this problem, the surface energy of the micromachine material must be reduced.[2,3] It has been suggested that coating the surfaces of micromachines with organic monolayers may be one way to overcome stiction.[3−6] This is one of the reasons behind the intense recent interest in self-assembled monolayers (SAMs) and Langmuir−Blodgett (LB) films as boundary layer lubricants.

In applications that involve solid surfaces in sliding contact adhesion of the molecules to the substrate is of paramount importance.[4] Thus, molecules that are covalently bonded to the substrate, such as those formed from self-assembly, are better candidates for boundary-layer lubricants than LB films. As a result, the molecular structure, mechanical properties, and tribological properties of SAMs have been studied a great deal using scanning probe microscopies.[7−23] Because alkanethiols on Au(111) are among the best characterized SAM systems,[24−32] they have been the subject of intense study for their value as boundary layer lubricants.

(1) Mastrangelo, C. H. Surface Force Induced Failures in Microelectromechanical Systems. In *Tribology Issues and Opportunities in MEMS*; Bhushan, B., Ed.; Kluwer Academic Publishers: Norwell, MA, 1998.

(2) Houston, M. R.; Howe, R. T.; Komvopoulos, K.; Maboudian, R. *Mater. Res. Soc. Sym. Proc.* **1995**, *383*, 391−402.

(3) Maboudian, R. *Mater. Res. Soc. Bull.* **1998**, *23*, 47−51.

(4) Dugger, M. T.; Senft, D. C.; Nelson, G. C. Friction and Durability of Chemisorbed Organic Lubricants for MEMS. In *Microstructure and Tribology of Polymer Surfaces*; Tsukruk, V. V., Wahl, K. J., Eds.; American Chemical Society: Washington, DC, 1999.

(5) Tsukruk, V. V.; Nguyen, T.; Lemieux, M.; Hazel, J.; Weber, W. H.; Shevchenko, V. V.; Klimenko, N.; Sheludko, E. Tribological Properties of Modified MEMS Surfaces. In *Tribology Issues and Opportunities in MEMS*; Kluwer Academic Publishers: Dordrecht, Boston, London: 1998; pp 607−614.

(6) deBoer, M. P.; Knapp, J. A.; Mayer, T. M.; Michalske, T. A. SPIE/EOS Conference on Microsystems Metrology and Inspection, Munich, Germany, 1999; http://www.mdl.sandia.gov/micromachine/docs/SPIE.0699.pdf.

(7) Barrena, E.; Ocal, C.; Salmeron, M. *J. Chem. Phys.* **2000**, *113*, 2413−2418.

(8) Beake, B. D.; Leggett, G. J. *Langmuir* **2000**, *16*, 735−739.

(9) Cooper, E.; Leggett, G. J. *Langmuir* **1999**, *15*, 1024−1032.

(10) Lee, S.; Shon, Y.-S.; Colorado, R.; Guenard, R. L.; Lee, T. R.; Perry, S. S. *Langmuir* **2000**, *16*, 2220−2224.

(11) Shon, Y.-S.; Lee, S.; Colorado, R.; Perry, S. S.; Lee, T. R. *J. Am. Chem. Soc.* **2000**, *122*, 7556−7563.

(12) Beake, B. D.; Leggett, G. J. *Phys. Chem. Chem. Phys.* **1999**, *1*, 3345−3350.

(13) Burns, A. R.; Houston, J. E.; Carpick, R. W.; Michalske, T. A. *Phys. Rev. Lett.* **1999**, *82*, 1181−1184.

(14) Barrena, E.; Kopta, S.; Ogletree, D. F.; Charych, D. H.; Salmeron, M. *Phys. Rev. Lett.* **1999**, *82*, 2880−2883.

(15) Barrena, E.; Ocal, C.; Salmeron, M. *J. Chem. Phys.* **1999**, *111*, 9797−9802.

(16) Kim, H. I.; Graupe, M.; Oloba, O.; Doini, T.; Imaduddin, S.; Lee, T. R.; Perry, S. S. *Langmuir* **1999**, *15*, 3179- -3185.

(17) Wong, S.-S.; Takano, H.; Porter, M. D. *Anal. Chem.* **1998**, *70*, 5200−5212.

(18) Harrison, J. A.; Perry, S. S. *MRS Bull.* **1998**, *23*, 27−31.

(19) Lio, A.; Charych, D. H.; Salmeron, M. *J. Phys. Chem. B* **1997**, *101*, 3800−3805.

(20) Lio, A.; Morant, C.; Ogletree, D.; Salmeron, M. *J. Phys. Chem. B* **1997**, *101*, 4767−4773.

(21) Carpick, R. W.; Salmeron, M. *Chem. Rev.* **1997**, *97*, 1163−1194 and references therein.

(22) Kim, H. I.; Koini, T.; Lee, T. R.; Perry, S. S. *Langmuir* **1997**, *13*, 7192−7196.

(23) Xiao, X.; Hu, J.; Charych, D. H.; Salmeron, M. *Langmuir* **1996**, *12*, 235−237.

(24) Fenter, P.; Eisenberger, P.; Liang, K. S. *Phys. Rev. Lett.* **1993**, *70*, 2447.

(25) Fenter, P.; Eberhardt, A.; Eisenberger, P. *Science* **1994**, *266*, 1216.

(26) Camillone, N.; Chidsey, C. E. D.; y. Liu, G.; Scoles, G. J. *J. Chem. Phys.* **1991**, *94*, 8493−8502.

(27) Dubois, L. H.; Zegarski, B. R.; Nuzzo, R. G. *Annu. Rev. Phys. Chem.* **1992**, *43*, 437.

(28) Dubois, L. H.; Zegarski, B. R.; Nuzzo, R. G. *J. Chem. Phys.* **1993**, *98*, 678−688.

(29) Poirier, G. E.; Tarlov, M. J.; Rushmeirer, H. E. *Langmuir* **1994**, *10*, 3383.

(30) Schreiber, F.; Eberhardt, A.; Leung, T. Y. B.; Schwartz, P.; Wetterer, S. M.; Lavrich, D. J.; Berman, L.; Fenter, P.; Eisenberger, P.; Scoles, G. *Phys. Rev. B.* **1998**, *57*, 12476−12481.

(31) Poirier, G. E. *Langmuir* **1999**, *15*, 1167−1175.

10.1021/ja010189u
Published on Web 06/21/2001

Theoretical simulations have also been used to examine the structure[33−38] and compression of *n*-alkanethiols on Au.[36,39,40] Previously, we have used MD simulations to examine the indentation[41] and friction[42−44] of SAMs composed of *n*-alkane chains of various lengths. In this work, we examine the effect of packing density on the frictional properties of alkane SAMs. Simulations of the type presented can be difficult to interpret because computational constraints require the use of periodic boundary conditions for a limited number of small systems over short periods of time. Despite this difficulty, it is still possible to meaningfully compare the qualitative results of these simulations with experimental measurements. Under load, the structure of tightly packed *n*-alkane monolayers is significantly different from loosely packed systems. These differences in structure lead to higher friction under high loads for the loosely packed system. This is in qualitative agreement with recent experimental work by Perry and co-workers.[10]

Methods and Procedures

The simulation systems consist of a diamond counterface that is brought into sliding contact with C_{18} *n*-alkane chains that are covalently bound to the (111) face of a diamond substrate. In the tightly packed system, the alkane chains are attached to the substrate in a (2×2) arrangement so that the density of the 72 chains is approximately the same as it is for alkanethiols on Au(111) (21.9 Å^2 per monomer).[19,25] The dihedral angles of the carbon backbones of alkane chains are initially in their *anti* configuration. The loosely packed monolayer is created by randomly removing 20 chains from the tightly packed monolayer.

Each layer of diamond in the simulation contains 288 carbon atoms. The diamond substrate and the diamond counterface each contain 13 layers of carbon atoms. The diamond counterface is hydrogen terminated to satisfy the valence requirements of carbon. Periodic boundary conditions are applied in the plane of contact between the probe and the sample and the dimensions of the computation cell in this plane are approximately 30.2 by 52.3 Å. The application of period boundary conditions means that this geometry models an infinite counterface. Thus, only compression of the monolayer, as opposed to penetration into the monolayer, is possible. Similar studies using a single-wall nanotube probe have been conducted to emphasize penetration into the monolayer;[41,43] however, nanotubes have much smaller contact areas than conventional AFM tips. It would be desirable to use a probe that is between these two extremes although this would require simulations with a much larger computational cell. At present, computational constraints prevent such an undertaking.

Atoms in the simulation are partitioned in the following way. The bottom two layers of the diamond substrate and top two layers of the counterface are held rigid (Figure 1). Moving inward toward the monolayer, the next two layers of the diamond substrate and the counterface are maintained at a constant temperature (300 K) using Langevin thermostats to simulate coupling with an external heat bath.[45] All remaining atoms are free to move according to classical dynamics. The equations of motion for all nonrigid atoms are integrated using the velocity Verlet algorithm with a constant step size of 0.25 fs.[46]

The force on each atom is derived from an adaptation of Brenner's reactive empirical bond-order (REBO) potential.[47,48] In this new potential, the adaptive intermolecular reactive empirical bond-order (AIREBO) potential,[49] a novel adaptive algorithm is used to introduce nonbonded interactions into the REBO potential without compromising its ability to model chemical reactions. Because this potential energy function can model chemical reactions, events such as wear and tribochemistry are possible in these simulations.

Compression of the hydrocarbon monolayers is accomplished by moving the rigid layer of the counterface at a constant velocity of 100 m/s toward the monolayer surface. Sliding of the counterface is accomplished by moving the same atoms at a constant velocity of 100 m/s along the direction of chain tilt (left to right in Figure 1). The load and friction force are taken to be the forces perpendicular to the monolayer and parallel to the sliding direction on the counterface.

Due to the complexity and range of the AIREBO potential, simulation sliding and compression speeds are limited to be on the order of 100 m/s. This speed is many orders of magnitude greater than the 10^{-8} m/s speeds typically used in nanoindentation experiments[18,21] and still several orders of magnitude greater than the 10^{-1} m/s speeds commonly used in AFM tapping mode. Additional comments regarding the sliding speed and its relationship to the dissipation of energy by various modes of motion are contained later in this work.

Results and Discussion

Friction force as a function of load is shown in Figure 2 for both of the C_{18} monolayers investigated. Each point represents the average friction force for a single 34.8 Å slide of the diamond counterface. Error bars are calculated by partitioning the slide into four, (2×2) unit-cell segments, which are 8.7 Å in length. Over the four bins, the friction force shows no systematic variation although load does show a systematic drop (typically less than 1%). To eliminate the influence of startup effects due to the abrupt transition between compression and sliding, the counterface is slid for 5 Å prior to beginning the first unit-cell segment. All slides for a given system originate from the single compression of one starting configuration. Thus, the error bars are indicative of the fluctuations that occur within a single slide but not indicative of fluctuations that can occur over a set of independently prepared starting configurations. Computational constraints force the calculation of error bars in this fashion.

The examined range of loads, 100−900 nN, corresponds to pressures in the range of 6−60 GPa. While a load of 60 GPa may seem extremely high, the diamond probe and substrate are infinitely flat without any imperfections; consequently, these systems are able to sustain very high loads without showing appreciable distortion of the diamond lattice. Furthermore, AFM experiments which look at atomic-scale friction typically report relative measurements between prepared systems due to difficulties in determining an absolute calibration of the atomic force microscope (both forces and area of contact).

Two Regimes. Analysis of Figure 2 suggests that there are two load regimes: a low-load regime (two low-load points), where the friction is independent of packing density and thus

(32) Woodward, J. T.; Walker, M. L.; Meuse, C. W.; Vanderah, D. J.; Poirier, G. E.; Plant, A. L. *Langmuir* **200**, *16*, 5347−5353.
(33) Mar, W.; Klein, M. L. *Langmuir* **1994**, 10, 188−196.
(34) Bhatia, R.; Garrison, B. J. *Langmuir* **1997**, *13*, 765−769.
(35) Bhatia, R.; Garrison, B. J. *Langmuir* **1997**, *13*, 4038−4043.
(36) Bonner, T.; Baratoff, A. *Surf. Sci.* **1997**, 377−379, 1082−1086.
(37) Luedtke, W. D.; Landman, U. *J. Phys. Chem.* **1998**, *102*, 6566−6572.
(38) Stevens, M. J. *Langmuir* **1999**, *15*, 2773−2778.
(39) Tupper, K. J.; Colton, R. J.; Brenner, D. W. *Langmuir* **1994**, *10*, 2041−2043.
(40) Tupper, K. J.; Brenner, D. W. *Langmuir* **1994**, *10*, 2335−2338.
(41) Tutein, A. B.; Stuart, S. J.; Harrison, J. A. J. *Phys. Chem. B* **1999**, *103*, 11357−11365.
(42) Tutein, A. B.; Stuart, S. J.; Harrison, J. A. *Langmuir* **2000**, *16*, 291−296.
(43) Harrison, J. A.; Mikulski, P. T.; Stuart, S. J.; Tutein, A. B. Dependence of Frictional Properties of Hydrocarbon Chains on Tip Contact Area. In *Nanotribology: Critical Assessment and Research Needs*; Kluwer Academic Publishers: Norwell, MA, in press.
(44) Mikulski, P. T.; Harrison, J. A. *Tribol. Lett.* **2001**, *10*, 29−38.
(45) Adelman, S. A.; Doll, J. D. *J. Chem. Phys.* **1976**, *64*, 2375−2388.
(46) Swope, W. C.; Andersen, H. C.; Berens, P. H.; Wilson, K. R. *J. Chem. Phys.* **1982**, *76*, 637- -649.
(47) Brenner, D. W. *Phys. Rev. B: Condens. Matter* **1990**, *42*, 9458−9471.
(48) Brenner, D. W.; Harrison, J. A.; Colton, R. J.; White, C. T. *Thin Solid Films* **1991**, *206*, 220−223.
(49) Stuart, S. J.; Tutein, A. B.; Harrison, J. A. *J. Chem. Phys.* **2000**, *112*, 6472−6486.

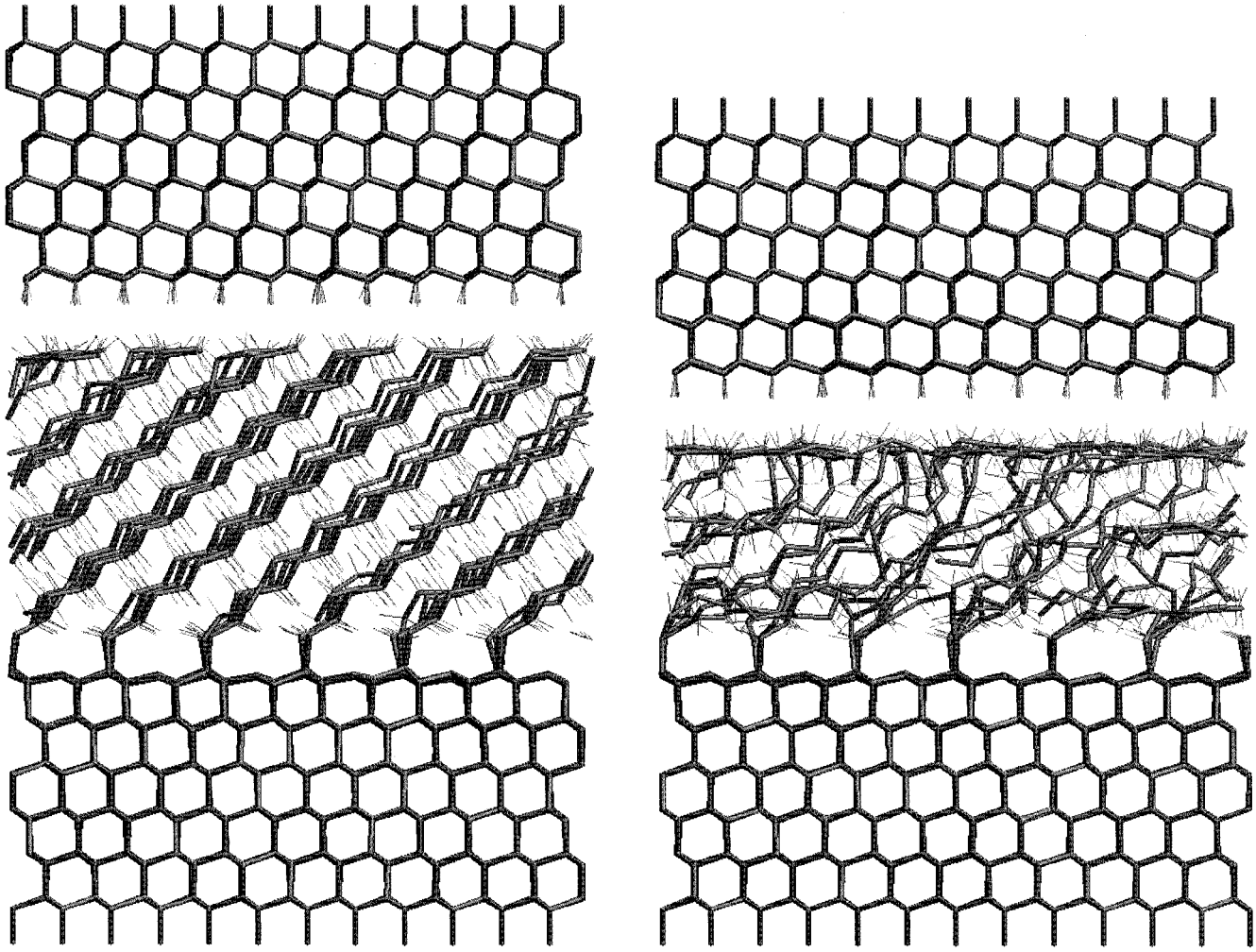

Figure 1. Conformations of the tightly packed monolayer (left) and the loosely packed monolayer (right) under a load of approximately 500 nN. The sliding direction is from left to right. Carbon atoms are shown in a gray-wireframe format and hydrogen atoms are shown in a thinner wireframe format.

insensitive to the structure of the monolayer, and a high-load regime (three high-load points), where the tightly packed monolayer gives a significantly lower friction at a given load.

The presence of two regimes is hinted at in the compression phase of the simulations. The volume per chain as a function of load is shown in Figure 3. The total volume of the chains is taken to be $A(z_{top} - z_{bottom})$ where A is the cross-sectional area in the plane and z_{top} and z_{bottom} are positions of the top and bottom of the monolayer. There are a number of ways to define z_{top} and z_{bottom}. All reasonable definitions that place z_{top} between the counterface and the monolayer and z_{bottom} between the monolayer and the substrate yield the same trends. The loosely packed monolayer has a large volume per chain initially. However, the application of any appreciable load decreases the volume as the chains undergo conformational changes to fill the vacant spaces caused by the removal of chains from the original (2×2) arrangement. The flexibility of the chains is also apparent from the presence of larger volume fluctuations at low loads (chains can move closer to, or farther away from, neighboring chains without appreciably changing the resulting load). In contrast, the volume per chain is highly constrained in the high-load regime. The chains are pinned in their relative orientation, and a small increase in the compression results in a large increase in the load. For the tightly packed system, Figure 3 suggests that the highly constrained volume sets in fully above about 300 nN.

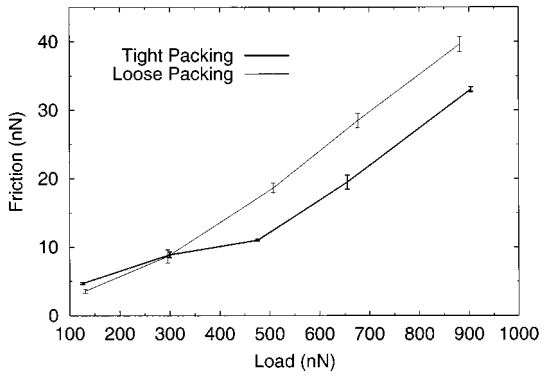

Figure 2. Friction as a function of load when a hydrogen-terminated counterface is in sliding contact with C_{18} hydrocarbon monolayers. Lines are drawn to aid the eye.

The form of the friction force of the tightly packed monolayer also manifests a change when transitioning from the low-load to the high-load regime. Figure 4 shows friction as a function of unit-cell bin position for slides conducted at loads near the transition region. For each slide, the four (2×2) unit-cell bins are superimposed and averaged. At the lower load ($\sim$300 nN), the tightly packed chains accommodate the sliding counterface by moving synchronously from side to side, resulting in a large-amplitude periodic variation of the friction. This behavior has

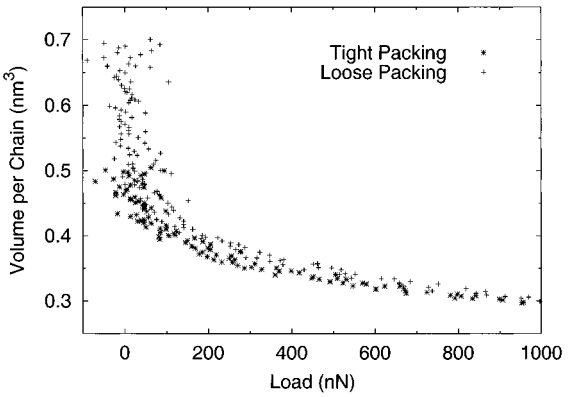

Figure 3. Volume of the monolayer divided by the number of chains as a function of load for the tightly (*) and loosely (+) packed monolayer. The top of the monolayer is taken to be the average between the highest atom from the chains and the lowest atom from the counterface. Likewise, the bottom of the monolayer is taken to be the lowest atom from the chains and the highest atom from the substrate.

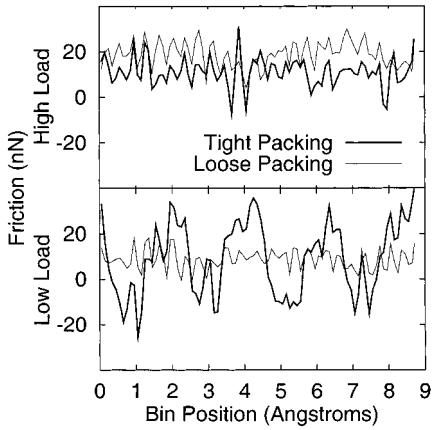

Figure 4. Frictional force as a function of sliding time for the loosely packed (light line) and tightly packed (heavy line) monolayers at loads near 300 nN (lower panel) and 500 nN (upper panel). The four unit-cell segments of each slide were superimposed by translating the sample time to a bin position. To reduce some of the small-scale fluctuations, each point on the curves represents an average over 80 samplings (20 from each unit-cell segment).

been examined in detail for a similarly prepared tightly packed C_{13} monolayer.[44] Essentially, the commensurate geometry of the hydrogen-terminated (1×1) counterface results in all of the chains being pushed to the same side in response to the approach of a subset of the terminal hydrogen atoms (the subset comprises one-fourth of the total number of hydrogen atoms due to the (1×1) arrangement of atoms on the counterface and the (2×2) arrangement of alkane chains). The next subset of hydrogen atoms pushes the chains back. Thus, each extrema in the periodic friction data in Figure 4 corresponds to an interaction with a subset of hydrogen atoms. The friction is high as any given subset approaches; as a subset recedes, friction can even go negative as the chains push the counterface along. The disorder of the loosely packed monolayer does not allow for this kind of synchronized behavior. However, this seems to have little effect on the average friction in this regime (as the average friction and load for these two slides are similar).

At the next higher load (~500 nN), the highly constrained volume suppresses the large-amplitude periodic variation in the friction observed in the tightly packed monolayer. Consequently, it is difficult to discern the difference between tightly and loosely packed monolayers by the shapes of the friction data shown in Figure 4. In this load regime, however, the average friction for tightly packed monolayer is significantly lower (~10 nN) than the loosely packed monolayer. This 10 nN difference in the average friction is maintained throughout the high-load regime. That is, the slopes of the friction versus load data of the two systems in the high-load regime are approximately the same.

Figure 1 shows snapshots of the two systems under a load that is just above the transition region. The basic geometries shown in this figure remain intact during sliding. There are only slight changes in positions that accommodate the sliding counterface. It should be noted that in the high-load regime, small changes in geometry can have large effects on the forces between the counterface and the monolayer. The disappearance of the large periodic fluctuations in the friction for the tightly packed monolayer indicate that the pinned chains can only respond slightly to accommodate the above counterface. Furthermore, those changes reflect more the local environment of each chain. In other words, while the average friction over the entire counterface does not vary a great deal over the slide, there are likely to be large variations in local forces.

The environment of the interface between the monolayer and the counterface is most likely controlled by both the order and the volume of the monolayer. Because the load is an approximate function of monolayer density, monolayer volume is roughly a function of the load and the number of chains. Thus, the loosely packed monolayer is of lower total volume for a given load (Figure 1). The disorder of the loosely packed monolayer, combined with the sensitivity of load to monolayer density, suggests that the load distribution over the counterface is uneven. During compression of the loosely packed monolayer, it is likely that potential barriers quickly grow, preventing the disordered monolayer from falling into a state which more evenly distributes the load. An uneven load distribution is likely accompanied by an uneven distribution in friction when sliding, possibly resulting in an overall higher friction relative to that of the more uniform tightly packed monolayer.

While the motion of chains is constrained at all loads in both monolayers, this effect is exacerbated in the tightly packed monolayer under high loads. This is evident in the scatter plots of Figures 5 and 6. In these scatter plots, the in-plane positions of the topmost carbon atoms of the chains are plotted as the sliding progresses for the loads near the transition region. It is clear from the size of "islands" that the tightly packed monolayer undergoes a transition to a more confined state in the high-load regime. In contrast, the loosely packed monolayer is characterized by a similar range of motion at all loads. These trends are confirmed by a calculation of average root-mean-square deviations for the in-plane positions of the topmost carbon atoms: there is a clear transition in the tightly packed monolayer that is not present in the loosely packed monolayer. It is in this transition region that the friction-versus-load data exhibit a change in slope (Figure 2). In contrast, the loosely packed monolayer maintains a similar range of motion at all loads, and the friction-versus-load data can be described by a single slope. This suggests that a large range of movement is accompanied by a large number of channels for energy dissipation, and thus high friction.

The coherent motion of chains in the tightly packed system at low loads (Figure 4) reflects the large range of motion because it is over this range of movement that the periodic structure of the probe is evident. At higher loads, efficient packing of the chains results in the confined geometry. On this smaller scale, the hydrogen atoms which terminate the probe do not maintain a relative order, and therefore the coherent motion is lost. However, it is the range of motion rather than the presence of

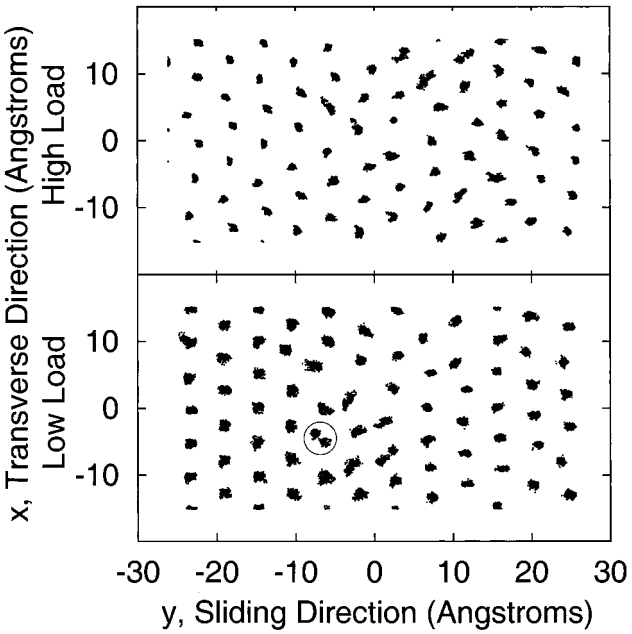

Figure 5. Position of the terminal carbon atom of the C_{18} chains during the 40 Å sliding run for the *tightly* packed monolayer below (lower panel) and above (upper panel) the transition region. The average load during the sliding run is approximately 500 and 300 nN in the upper and lower panels, respectively. Circle represents a "double-island" site referred to in the text.

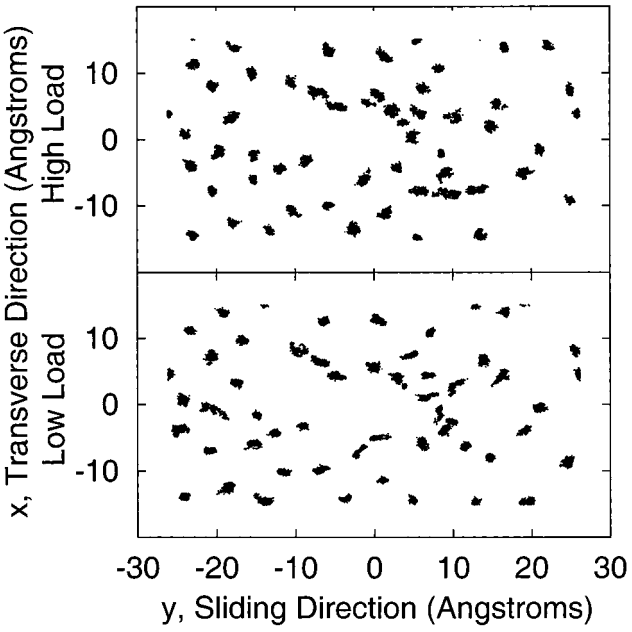

Figure 6. Position of the terminal carbon atom of the C_{18} chains during the 40 Å sliding run for the *loosely* packed monolayer below (lower panel) and above (upper panel) the transition region. The average load during the sliding run is approximately 500 and 300 nN in the upper and lower panels, respectively.

coherent or incoherent motion which connects the observed properties of the tightly packed system with those of the loosely packed system.

The scatter plots of Figures 5 and 6 also demonstrate that, in large part, the motion each chain tip undergoes is localized (the motion of the end of the chain defines an "island"). However, there are a few cases where a chain tip "jumps" from one island to a nearby island. These jumps are likely indicative of high-stress regions that develop during sliding. In the tightly packed monolayer, this is supported by the fact that the region surrounding the double island sites (circled in Figure 5) is more disordered than the regions far from these sites where the (2×2) packing arrangement of the chains is clearly evident. Furthermore, comparisons of the relative orientation of carbon atoms in a monolayer under load indicate that the relative geometry is largely maintained as the load is increased. It is also the case that once a jump occurs, no jumps back have been observed during the remainder of the slides. These trends suggest that jumps require large local forces that significantly alter local geometry. Currently, it is not clear whether this sort of "jumping" occurs in AFM experiments or is unique to the simulations.

Gauche Defects and Energy Dissipation. The tightly packed monolayer is more ordered near the surface not only due to the efficiency of the packing but also because the chains have an even number of carbon atoms (even-terminated). In this case, the last carbon−carbon bond in each chain is naturally pointed primarily in the sliding direction. In contrast, when not under load, in chains with an odd number of carbon atoms (odd-terminated) the terminal carbon−carbon bond is predominately pointed upward (out of the monolayer plane).[41,42,44] Simulations show that under the application of a load this terminal carbon−carbon bond is pushed down to one side or the other in a direction that is in the plane but not aligned with the sliding direction.[44] As an even-terminated monolayer is compressed, chain tilt increases, however, the basic configuration of the surface remains ordered with the terminal bond remaining pointed in the sliding-direction.

In addition, the formation of terminal gauche defects (defects on the ends of the chains) is inhibited in systems with an even number of carbon atoms in the alkane chains. Salmeron has discussed the possibility that *terminal* gauche defects may play a small role in energy dissipation (he notes that *internal* gauche defects are difficult to excite in well-packed layers) because energy is required to change the torsional angle associated with the last four carbon atoms in the chain.[50] This seems plausible in the case of the odd-terminated chains because the formation of the defect also reduces the height of the monolayer. However, such changes in the torsional angles for the even-terminated chains are difficult to achieve with the counterface probe. The formation of gauche defects, primarily defects associated with the terminal carbon atoms but also defects deeper in the monolayer, might play a more significant role in simulations that account for edge effects of the probe.[41] The flat counterface utilized in this study is infinite in extent, and thus it is only capable of compressing the monolayer.[42,44] The slight fluctuations in the height of the surface carbon atoms of the monolayer that are evident in the simulations presented here are only a response to small periodic variation in the counterface due to the terminating hydrogen atoms. Simulations that utilize a probe with some curvature would more likely address the importance of gauche defect formation because the heights of the chains during a slide would vary significantly as chains are pushed under and emerge from under the probe. In fact, previous simulations that utilized a finite-sized tip, that is, a single-wall carbon nanotube, demonstrated that these tips are able to penetrate the monolayers and thus cause defects to form deeper within the monolayer.[43] To date, no friction measurements have been made with a tip that has an area of contact that is comparable to the single-wall nanotube used in those simulations. The radius of a typical AFM tip is approximately 100−500 Å. With a radius of this size, there is a significant flat region

(50) Salmeron, M. *Tribol. Lett.* **2001**, *10*, 69−79.

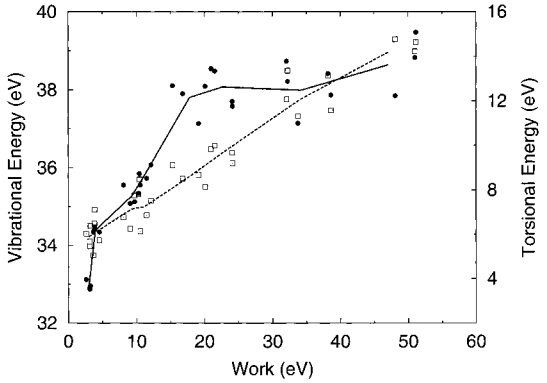

Figure 7. Vibrational (open squares) and approximate torsional (filled circles) energy as a function of work for a monolayer of *tightly* packed C_{13} chains. These runs were conducted as reported in ref 44.

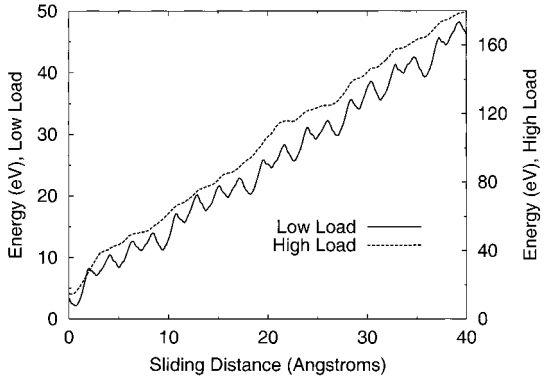

Figure 8. Total energy (including the energy being pulled out by the thermal bath) as a function of sliding time for a system of *tightly* packed C_{13} chains at low (solid line) and high (dashed line) load. The loads are 100 and 400 for the low- and high-load runs, respectively. These runs were conducted as reported in ref 44.

under the tip where many chains stay compressed over a length scale longer than the thickness of the monolayer. The present simulations are aimed at addressing this region without the computational burden of treating edge effects. While it is the case that gauche-type defects are evident in the present simulations even in the case of tight packing (although the numbers are small), it is not clear that they play a significant role with respect to energy dissipation and friction.

Previous sliding simulations that have probed the friction of C_{13} alkane chains in a (2×2) arrangement with a counterface have shown a correlation between the number of gauche defects and the frictional force.[42] A more detailed examination of this system under slightly different conditions demonstrated that the correlation of gauche defects with friction was a consequence of the correlated motion of the chains.[44] (In that work, the constraint of a rigid counterface was imposed to simplify the tracking of energy flow.)

Those simulations on C_{13} alkane chains also demonstrated that while gauche-defect generation reflects energy changes at the monolayer surface (ends of the chains), this does not appear to be a significant channel for the dissipation of energy in a system with this geometry. This is apparent from analysis of a plot of vibrational energy and approximate torsional energy as a function of the work done by the sliding counterface (Figure 7). The results for eight slides at different loads are shown. As with the C_{18} systems above, each simulation is divided into an initial 5 Å segment which is not analyzed, followed by four unit-cell bins. Each data point (32 data points total) in Figure 7 corresponds to one of the bins for a single slide (lines follow the average over the four bin segments). The work is done by the counterface on the sample over the unit-cell slide. Because the counterface is rigid and sliding at constant speed, the work is proportional to the friction. The vibrational energy is that associated with the carbon backbone of the chains, and the torsional energy is the approximate energy associated with the torsional angles in the carbon backbone of the chains. The approximate torsional energy is calculated by mapping the torsional angle of each set of four consecutive carbon atoms from the backbone of a chain to the potential energy of a corresponding uncompressed butane molecule with the same torsional angle (the energy minimum of the butane molecule is taken to be zero). While these two quantities do not take into account all possible modes of energy flow, some important trends are evident.

Initially both vibrational energy and approximate torsional energy rise with the work (and thus the friction). However, while the vibrational energy continues to rise linearly as the load is increased, the torsional energy reaches a plateau. This regime where the torsional energy flattens out is analogous to the transition region in the C_{18} runs. This is also apparent in Figure 8, which shows the total system energy (including the energy stored in the thermal bath) as a function of sliding time for two slides, one under low load and one under high load. Under low load, the motion of the chains is periodic, and this is reflected in the periodic structure of the system energy (and the frictional force as in the C_{18} system). There is an overall linear rise in the total energy as energy builds up in the thermal bath, but there are segments where the correlated movement of the chains pushes the counterface along (where the slope of the system energy is negative). Under high load, the monolayer is more disordered and confined, and the system energy rises steeply. There is still some periodic structure although it is not nearly so obvious as in the low-load case. Some periodic structure is expected because uncorrelated movement of the hydrogen atoms that terminate the counterface is not possible when the probe is held rigid. Furthermore, there may be effects associated with the geometry of odd-terminated chains that are not present in the even-terminated systems as seen in SPM experiments.[17,51] The presence of two load regimes that exhibit qualitatively different behavior is in agreement with the observations made in the C_{18} sliding runs.

It is important to acknowledge the difficulty of assessing the contribution of gauche defects to the energy balance of the system. The method used to calculate the torsional energy implies that its contribution flattens out with increasing load. Thus, torsional energy and friction do not respond the same way to the application of load. This may mean that the generation of gauche defects is not a major channel of energy dissipation. There are several other possibilities, however. First, the torsional energy contribution is mapped to an uncompressed butane molecule. However, the configuration of individual chains is altered under the application of load; thus, it may not be appropriate to map the torsional angles to an uncompressed molecule. Furthermore, the result of the formation of a defect with respect to the surrounding region is untreated (it was shown above that changes in the orientation of a chain tip can significantly affect the order in its local region). Finally, the saturation, or flattening, of the torsional energy contribution may be related to the sliding speed. It is possible that the characteristic time required for a gauche defect to anneal is longer than the time between subsets of hydrogen atoms on the

(51) McDermott, M. T.; Green, J.-B. D.; Porter, M. D. *Langmuir* **1997**, *13*, 2504−2510.

counterface interacting with the ends of the chains. Thus, the number of defects would continue to increase, eventually reaching some constant level. To date, computational constraints have prevented simulations such as the ones presented here at slower sliding speeds. In short, the flattening of gauche energy says more about the number of gauche defects than about how much defects contribute energetically. It is possible that although the number of gauche defects flattens out in the high-load regime, the contribution of each defect energetically can still continue to rise.

This difficulty of trying to quantify gauche defects energetically reflects the difficulty of trying to connect any geometrical property of the monolayer with friction. The best approach lies in looking for strong correlations between the evolution of structural properties and instantaneous friction forces. While correlations between the number of gauche defects and average friction have been established for this type of probe (an infinite counterface) and sample (a linear hydrocarbon SAM), stronger correlations with other properties have been found (for example, see the discussion of bond length later in this work). It is perhaps important to note that, particularly in a system with a great deal of uniformity (the tightly packed monolayer), it is quite possible that properties correlated with friction are not necessarily the essential properties that give rise to the observed frictional behavior.

It is not surprising that the vibrational energy rises linearly with the rate at which work is done on the sample; energy must flow through the monolayer somehow, and it is certainly vibrational energy that characterizes the flow of energy through the diamond substrate. Extrapolating the linear rise in vibrational energy done to zero work, it is evident that there is significant heating of the monolayer due to the large sliding speed (about a 17% increase in the vibrational energy at the highest work rates). Vibration, however, is not the vehicle by which energy moves from the probe to the sample. The discussion below suggests that the stretching of chains is a means by which energy is transferred from the probe to the monolayer, although it will be necessary in future simulations to store information about the contact forces between the individual atoms of the probe and the collection of atoms comprising the sample to make more conclusive statements.

Monolayer Thickness and Chain Length. As noted above, the average load on the counterface is approximately a function of the density of atoms within the monolayer, independent of the characteristics of the monolayer. Because the loosely packed system has approximately 30% fewer chains, the thickness of the loosely packed monolayer is about 30% less than the thickness of the tightly packed monolayer under similar loads (Figure 1).

Examination of a number of properties (position of the end group, alignment of chains with sliding direction, and tilt angle of the chains) shows correlations between the geometric structure of the monolayer and the forces on the counterface.[44] A vivid example which shows clearly that entire chains in the tightly packed monolayer respond to the sliding counterface and not just the region near the surface is depicted in Figure 9. In this figure, the friction and the average chain length as a function of time in the low-load regime are shown for a slide across the tightly packed monolayer. The chain length is defined as the distance along the carbon backbone starting from the bottom-most carbon atom in the chain and going to the topmost carbon atom. In other words, dividing the average chain length by ($N - 1$), where N is the number of carbon atoms per chain, gives the average bond length of carbon−carbon bonds in the

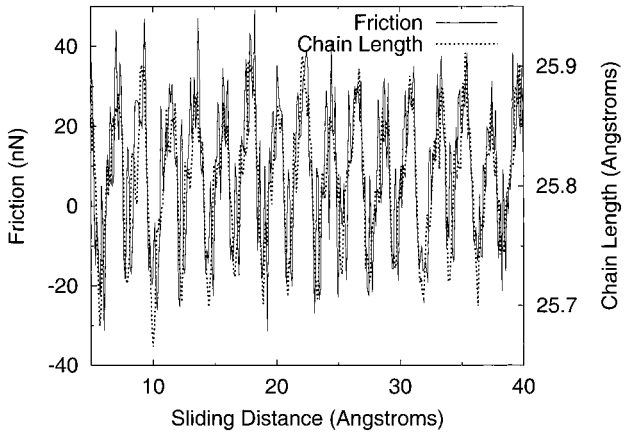

Figure 9. Frictional force (solid line) and change in carbon-backbone chain length (dashed line) as a function of sliding time for a system of *tightly* packed C_{18} chains. The load is below the transition region and corresponds to the point at approximately 300 nN in Figure 2.

monolayer. While the overall change in length is small, it is tightly correlated with the friction. It is clear that stress builds in the chain as the counterface stretches the chains. When the subset of hydrogen atoms from the counterface clear the chain tips, the chains spring back to a relaxed length. The process is then repeated as the next subset of hydrogen-counterface atoms encounters the chain tips. A look at the individual bond lengths along the chain backbones shows that this change in length is a response of the entire chain and is not associated with just the portion of the chain near the monolayer surface. Therefore, it is possible that a thicker monolayer (tightly packed) may provide additional cushion over which the accommodating adjustments to the counterface can be made, perhaps accounting for the trend of decreasing friction with increasing chain length observed in experiments.[19,21]

The use of the term "spring back" should not be taken too literally. Simulations that subtracted the sliding velocity vector from each atom in the probe at several points along one of the "spring back" segments were conducted. Although halting and equilibrating for 10 ps resulted in slight changes in geometry, the chains do not spring back to the shortest chain lengths. This suggests that the sliding speed utilized here may not be problematic; however, it will still be necessary to reduce sliding speeds by an order of magnitude before definitive statements can be made.

While many geometrical properties are correlated with friction, the correlation of friction with chain length is the strongest among those investigated. This strong correlation suggests that the bond lengths along chain backbones of the tightly packed and the loosely packed monolayers may show different trends. The data in Figures 10 and 11 demonstrate that this is in fact the case. In the lower panel of Figure 10, the average bond length is the average over all carbon−carbon bonds in a given monolayer and over the duration of the four bin sliding segments. A histogram of fluctuations in these bond lengths, where deviations are calculated for each bond about its average, is shown in the upper panel. Precisely, the differential probability, $p(l)$, is defined so that $p(l)\mathrm{d}l$ represents the probability that a randomly chosen bond at a randomly chosen time has a bond length that deviates an amount l from that bond's overall average over the four-bin sliding segments. The standard deviations of the lower panel are of these differential probability functions over both monolayers and all slides under load (the two points on the far right are for no load with increasing loads progressing to the right).

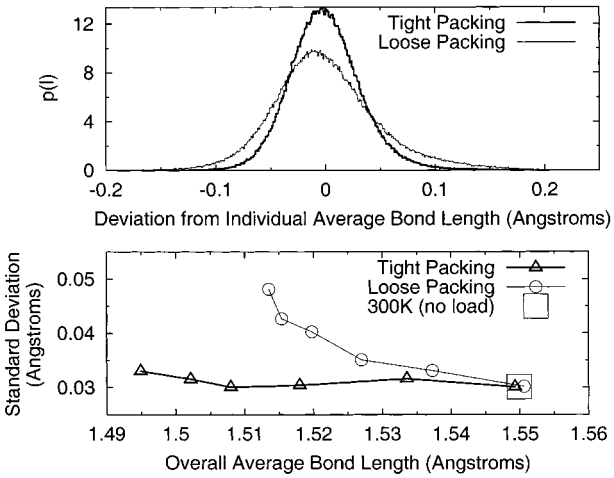

Figure 10. Upper panel: Histograms of deviations in bond lengths of all the carbon−carbon bonds in the monolayers from their averages. Deviations are calculated for each individual bond about its average over the same four-bin sliding segments used to calculate these data in Figure 2. The histograms have been scaled to a differential probability $p(l)$ which gives the probability $p(l)\mathrm{d}l$ that a bond chosen at random deviates from its average by an amount within l to $l + \mathrm{d}l$. The load is the highest examined for each system: 904 and 881 nN for tight and loose packing, respectively. Lower panel: The standard deviation of the deviations for each load plotted against the overall average bond length. Also shown is the result for each system under no load. Lines are drawn to aid the eye (higher loads correspond to shorter bond lengths).

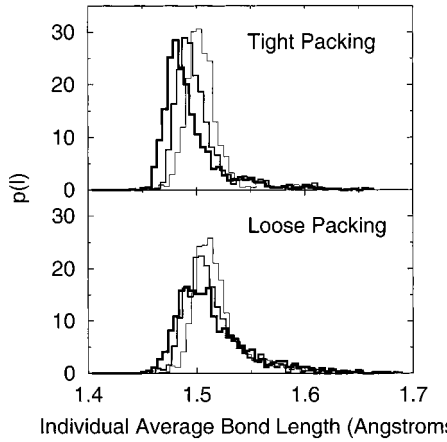

Figure 11. Histograms for the distribution of average carbon−carbon bond lengths within the monolayers for the three highest loads of each system. The highest load is given by the thickest line progressing to the lowest load of the high load regime which is given by the thinnest line. An average individual bond length is calculated by averaging the bond lengths of a single carbon−carbon bond in the monolayer over the four-bin sliding segments which total 349 samplings spaced by 0.1 Å. The histograms have been scaled to a differential probability $p(l)$ which gives the probability $p(l)\mathrm{d}l$ that a bond chosen at random has an average length within the l to $l + \mathrm{d}l$ (each histogram is of unit area).

It is clear that the efficient packing of the tightly packed monolayer permits a smooth compression: bond length decreases significantly for each progressively higher load. Furthermore, bond-length fluctuations stay very close to the thermal fluctuations which characterize the monolayer under no load (the width of these thermal fluctuations is much larger than the systematic change in bond length associated with the varying friction). This suggests that this monolayer is able to efficiently dissipate energy. In contrast, the average bond length decreases less and less with increasing load for the loosely packed monolayer. Accompanying this diminishing decrease in bond length is a significant increase in bond-length fluctuations. This suggests that the probe is channeling a great deal of energy into the vibration of bonds through the stretching of chains or possibly that the disordered structure of the monolayer inhibits the dissipation of energy out of the monolayer and into the diamond substrate.

The diminishing decrease in average bond length for the loosely packed monolayer, along with this monolayer's irregular structure, suggests that in response to sliding under larger load the average lengths of individual bonds are stretched in some regions, while compressed in other regions, depending on local environment. This would manifest itself as a greater spread in average bond lengths in a loosely packed monolayer versus a tightly packed monolayer under similar load.

Figure 11 compares the averages of individual bond lengths (all carbon−carbon bonds in the monolayer) in the tightly and loosely packed monolayers under the highest three loads. Because the histograms have been converted to represent the differential probability that an individual bond is characterized by a specified average length, the area under each curve is unity. Both monolayers show an overall trend toward shorter bond lengths under higher loads. However, it is clear that the loosely packed system is characterized by a wider spread in bond lengths. The much higher level of irregularity in the loosely packed system gives rise to a long bond-length tail, which does not compress under increasing load despite the fact that the volume of the monolayer is decreasing. This results in broader peaks in the differential probability at higher loads. In contrast, the shapes of the curves for the tightly packed monolayer are roughly the same except that the average decreases with increasing load. For the loosely packed monolayer, the wider spread in bond lengths is likely correlated with a high degree of nonuniformity in contact forces between the atoms of the probe and the sample. Under high load, this nonuniformity may explain the higher friction in comparison with that of the very regular ("smooth") tightly packed monolayer.

Sliding Direction. The linear rise in vibrational energy of the carbon backbones with friction (Figure 7) and stretching along the entire length of the backbones (Figure 9) suggest that the explanation of frictional properties and energy dissipation involve looking at how the entire tightly packed monolayer responds to the sliding counterface. The shape of the friction and chain length curves as a function of time also suggest that the sliding direction (along the tilt of the chains) may be important. In fact, slides conducted with the tightly packed system in directions along, against, and transverse to the tilt of the monolayer chains show that sliding direction can have an effect on the friction force, and that the friction force is closely connected with the compression and elongation of bonds along the carbon backbone of monolayer chains.[52]

Summary

Molecular dynamics simulations have been used to examine the effect of packing density of SAMs composed of *n*-alkane chains on friction. Tightly packed monolayers exhibit lower friction than loosely packed monolayers under high loads. At high loads, the motion of the chains in the tightly packed monolayer is restricted owing to the efficient packing and the ordered nature of the chains. Perry and co-workers used AFM to examine the friction and various surface science techniques to examine the crystalline order of SAMs derived from normal and spiroalkanedithiols.[10] In that work, they reported that loosely

(52) Mikulski, P. T.; Harrison, J. A. in preparation.

packed and disordered SAMs exhibit higher interfacial friction than those that are well-packed and highly ordered. While a direct comparison of data from our MD simulations with data from AFM experiments is problematic, due to differences in contact geometries and sliding speeds, the agreement is encouraging. The small "island" geometry of the tightly packed monolayers under high loads and the histograms of individual bond lengths shown in Figure 11 demonstrate that efficient packing and the application of load inhibits excessive stretch of the chains. This transition, which is not evident in the loosely packed system, is accompanied by a lessening of the slope of average friction versus load, thus possibly explaining the lower friction at high loads.

Salmeron and co-workers[19,23,50] have suggested that the generation of terminal gauche defects at the surface of monolayer films may lead to a small amount of energy dissipation. This work and previous simulations in our group[41−44] demonstrate that gauche defects do form and dissipate energy during sliding. However, for the infinitely flat contact geometry examined here, these defects are localized to the ends of the chains and their contribution plateaus as load increases. This may mean that gauche-defect generation is not a significant channel of energy dissipation. However, it is also possible that approximations used to extract the torsional energy do not capture the essential physics of problem. Furthermore, scanning speeds employed in AFM experiments are orders of magnitude slower than the sliding speeds used here. Thus, while torsional angle changes do not seem to be important in these simulations this channel of energy dissipation may increase in importance as the sliding speed decreases. These simulations show that once energy is transferred to the monolayer from the probe, it is channeled through the monolayer via vibration, which accounts for most of the energy lost during sliding at these speeds.

Previous simulations have shown that, when one uses a finite tip to indent the alkane chains, gauche defects form not only under the tip but also adjacent to it.[43] That is, the tip is able to penetrate the monolayer and form defects within the monolayer. These studies utilized a single-wall carbon nanotube, which is approximately an order of magnitude smaller than a conventional AFM tip, as a probe. Because AFM tips have a large contact area under the tip, they may respond in a way similar to that of the simulations that utilize the infinitely flat surface. Experimentally it is not clear the degree to which edge effects contribute to the measured friction. Our simulations suggest that the area under the tip may be the region that is primarily responsible for the measured friction. Computational constraints have thus far prevented the simulation of friction using tips comparable in size to those of AFM experiments.

Acknowledgment. This work was supported by the U.S. Office of Naval Research and by the Air Force Office of Scientific Research under Contracts N00014-01-WR-20213 and NMIPR-01-5203507, respectively.

JA010189U